https://ntrs.nasa.gov/search.jsp?R=19800010834 2020-03-21T20:02:59+00:00Z

79N17261

NASA TECHNICAL MEMORANDUM NASA TM-75718

STRUCTURAL ANALYSIS OF HOLLOW BLADES -- TORSIONAL STRESS ANALYSIS OF HOLLOW FAN BLADES FOR AIRCRAFT JET ENGINES

A. Ogawa, Y. Sofue and T. Isobe

(NASA-TM-75718) STRUCTURAL ANALYSIS OF HOLLOW BLADES: TORSIONAL STRESS ANALYSIS OF HOLLOW FAN BLADES FOR AIRCRAFT JET ENGINES (National Aeronautics and Space Administration) 25 p HC A02/MF A01 CSCL 21E G3/07

N80-19111

Unclas 47453

Translation of "chūkūyoku no kōzō kaiseki -- fan dōyoku no nejiri ōryoku kaiseki --," National Aerospace Laboratory, Tokyo, Japan, Report NAL-TR-533, May 1978, 15 pages

NATIONAL AERONAUTICS AND SPACE ADMINISTRATION
WASHINGTON, D. C. 20546 OCTOBER 1979

Structural Analysis of Hollow Blades
(Torsional Stress Analysis of Hollow Fan Blades for Aircraft Jet Engines)

By A. Ogawa, Y. Sofue and T. Isobe
National Aerospace Laboratory

1 Preface

/1*

In recent years the trend in fanjet engines has been to greater size and thrust, and in line with this the daimeter of fan blades has increased and, since out of considerations of strength and rigidity the fan chord length has also increased, there has been an overall trend to greater size. This enlargement of the fan blades necessarily led to the thickening of the fan shaft which must withstand the centrifugal forces, and the weight of other components is also increased by the same influences. Since such an increase in weight causes a considerable lowering of performance in the case of an engine for aircraft use, the hollowing of the fan blades becomes necessary. Experimental fan blades have already been tested in this laboratory with the aim of studying such light weight hollow blade construction to increase their trustworthiness in respect to structural strength [1,7]. Here we report the results of a study, using numerical analysis by the finite element method, of the effects of the hollowing of fan blades on strength and rigidity.

For the load, we have assumed a torque load arising from a component of the centrifugal force. Considering this a St Venant torsion problem, the method of analysis is numerical analysis by the finite element method, according to the procedures of Kawai and Yoshimura. On this occasion, partly to increase the refinement of the calculation and partly because of the complexity of the hollowed sections, a situation gradually developed in which the number of divisions exceeded one thousand. When the number of divisions became so

*Numbers in the margin indicate pagination in the original text.

large, the production of data and checking of errors became too much for human strength, so we decided to devise a two dimensional diagram automatic dividing program to make the process easier.

In order to obtain data for the hollowing configuration most suitable from the perspective of strength and torsional rigidity, we analyzed models in which reinforcing webs were placed in the hollowed section in varying numbers and locations.

As the result of investigation mainly concerning the location and number of webs in relation to torsional rigidity and the convergence of stresses, we have obtained data concerning the optimum locations for webs. From analysis of many models, we have obtained a forcast of 30% hollowing against torsional loadings.

2 Methods of Analysis

2.1 Load Distributions and the Modelling of Blades

The shape and dimensions of experimental fan blade F-10 are shown in Figure 1. In the distance of 260mm between blade root and blade tip there is a twist of about 37%. The fan blade can have a pin-joint coupling or a double tail coupling, and the bending moment /2 due to air pressure is calculated to be balanced by the centrifugal force.

Stress caused by torque as a component of centrifugal force principally arises in the fan blade [1]. Figure 2 shows the analysis of the torque.

In a case where the fan blade and the torque are as in Figures 1 and 2, then for a rigorous stress analysis a three dimensional elastic analysis would be necessary, but as an approximation we have analyzed the one face of the blade where the torque is greatest as a St Venant two dimensional torsion problem [2].

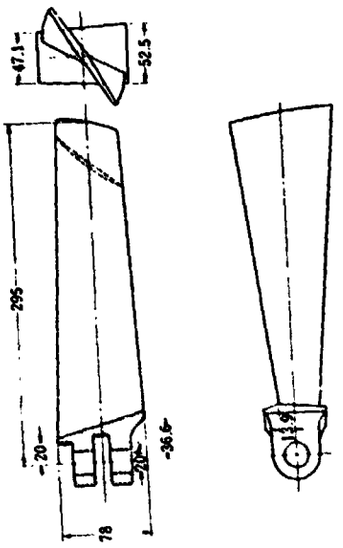

Figure 1. Experimental Fan Blade.

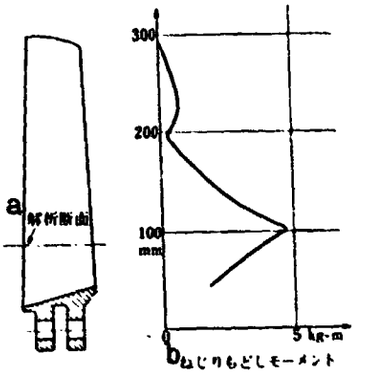

Figure 2. Torque Distribution.

Key: a cross section of analysis

b torque

We assumed the length of the fan blade to be infinite and the cross section uniform.

For this cross section we take a cross section of the fan blade at the location where the torque is greatest. And, since we take it that the effect of the fastening of the blade root is to increase rigidity, we consider that the result of the above mentioned treatment as a St Venant two dimensional problem will be a safe approach.

2.2 Configuration of the Hollow Blades

When establishing the configuration of the hollowing, one determines the percentage of hollowing as given in the following formula.

$$\text{percentage of hollowing} = \frac{\text{hollow cross section area}}{\text{blade cross section area (including hollow portion)}} \times 100$$

The result of an evaluation employing an approximate analysis by membrane theory is that in the case of such a model as in Figure 3, where the percentage of hollowing is made about 30%, the maximum stress will be less than 10kg/mm^2.

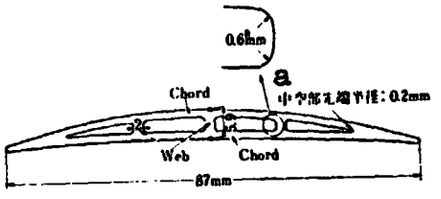

Figure 3. An Example of a Hollow Blade Model (material T_s alloy)

Key: a radius at tip of hollow section

From this we established the percentage of hollowing at 30%, and carried out analysis of the models shown in Table 1, where the number and location of reinforcing webs in the hollowed section were varied. In Table 1 the designation, number of elements, percentage of hollowing, and number of node points are shown for each analytical model. In Figure 4 (a)-(j), the configuration of each model is shown as a mosaic of triangular elements of the finite element method.

Since the cross section analyzed is symmetrical about the Y axis, analysis was carried out only for the right hand half.

The thickness of the reinforcing webs is 2mm, the radius of the joints between web and chord is 0.6mm and the radius of the tip of the hollowed section is 0.2mm, except in the case of the webless model OB. As the number of webs is increased, the thickness of the chord must be reduced slightly to keep the percentage of hollowing and the web thickness constant. Because of this, the situation must be considered in which a decrease in rigidity and an increase in stress due to the decrease in chord thickness which exceeds the reinforcing effect of the webs becomes a problem. The web thickness of 2mm was /4 selected in relation to considerations of manufacture.

Finally, the percentage of hollowing was intended to be 30%, but this became difficult to maintain uniformly due to the complexity of the configuration, and there is a variation of $\pm 1\%$.

ORIGINAL PAGE IS
OF POOR QUALITY

TABLE 1. THE ANALYTICAL MODELS

Number of Webs	Model	Description	Cross Section Area (mm)	Hollowing	Elements	Node Points
	Solid	solid model	367.08	0	233	153
0	0A	tip radius 0.16mm	255.92	30.28	713	457
	0B	" " 0.5mm	256.30	30.18	729	455
1	1A	web centered	255.40	30.42	921	568
2	2A	2 webs	253.56	30.93	963	586
	Opt	webs at optima	257.44	29.87	1229	734
3	3A	webs centered	257.82	29.76	1103	668
	3B	webs even	258.38	29.65	1103	668
	3C	webs near tips	257.98	29.72	1094	663
7	7A	7 webs	260.18	29.12	1453	868

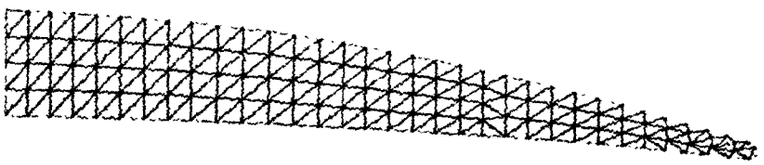

Figure 4(a). Solid Blade Model (solid)

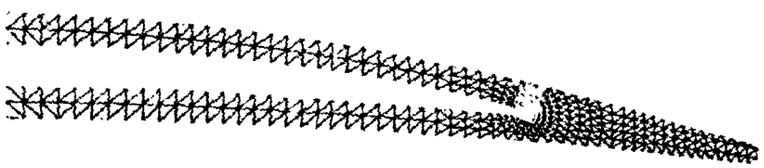

Figure 4(b). Webless Model (0A)

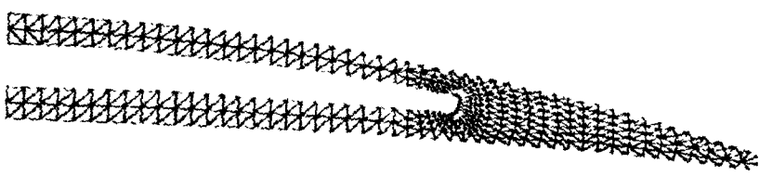

Figure 4(c). Webless Model (0B)

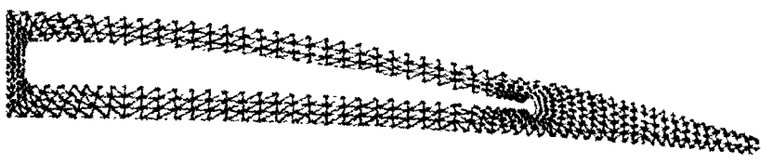

Figure 4(d). 1 Web Model (1A)

ORIGINAL PAGE IS OF POOR QUALITY

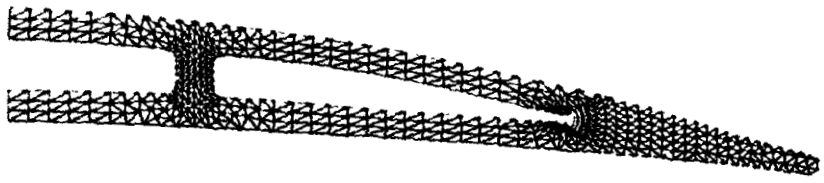

Figure 4(e). 2 Web Model (2A)

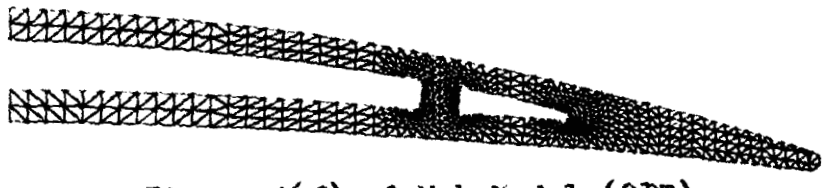

Figure 4(f). 2 Web Model (OPT)

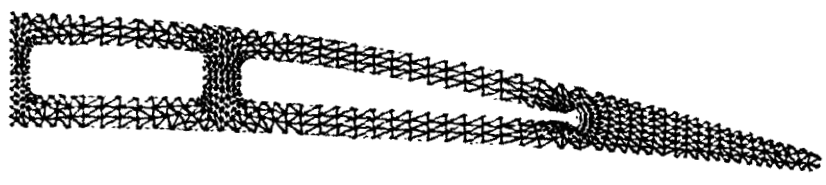

Figure 4(g). 3 Web Model (3A)

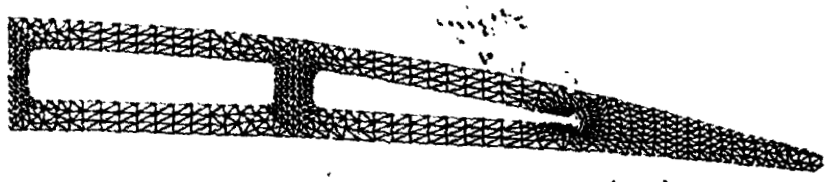

Figure 4(h). 3 Web Model (3B)

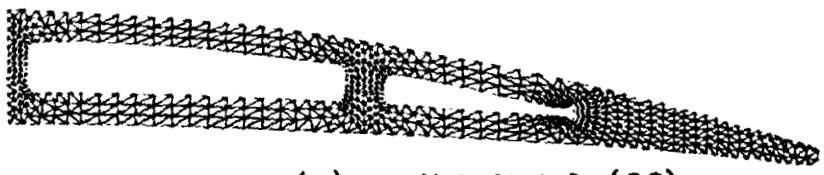

Figure 4(i). 3 Web Model (3C)

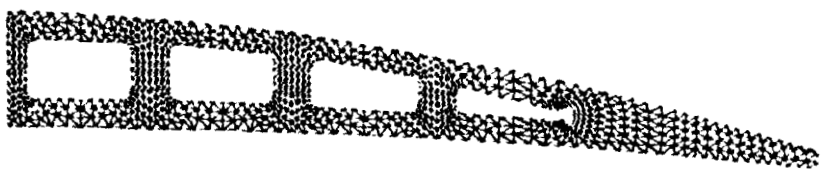

Figure 4(j). 7 Web Model (7A)

2.3 Technique of Two Dimension Torsional Stress Analysis using the Finite Element Method

/5

The problem of torsion across a bar of uniform cross section, based on the theory of St Venant, is solved by the method of Kawai [3]

Yoshimura using finite elements.

There is demarcated a section from the bar of uniform cross section of a length of 1 unit in the direction of the axis, as shown in Figure 5(a), and then a system of right angle coordinates is established, as in the figure. Next it is modelled as a mesh of triangular elements as shown in Figure 5(b).

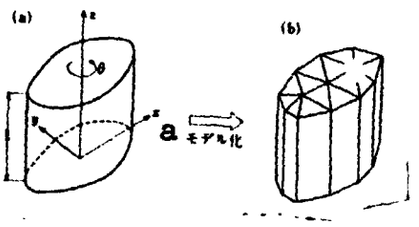

Figure 5. Modelling a Bar of Uniform Cross Section

Key: a modelling

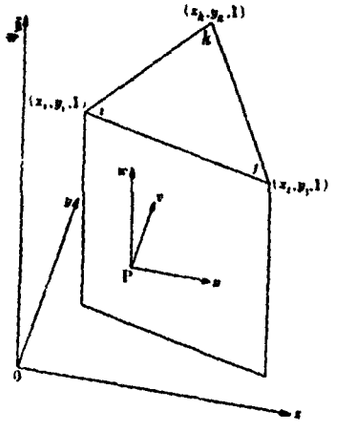

Figure 6. A Triangular Finite Element

A triangular element ijk is shown in Figure 6. The displacement (u,v,w) of a given point P within this element can be generally determined, according to St Venant's theory, as follows.

$$u = -\theta yz \qquad (2.1)$$

$$v = \theta xz \qquad (2.2)$$

$$w = h(x,y) \qquad (2.3)$$

Here θ is designated "percentage of torsion.

As is clear from the above equations, u and v of the given point P within the element may be determined directly from the x,y coordinates given θ, and so column vector $\boldsymbol{d}$ of the displacement of the the node point of a triangular finite element may be simplified to the following component.

$$\boldsymbol{d} = \{\theta, w_i, w_j, w_k\}^T \qquad (2.4)$$

(Here superscript T shows the displacement matrix.)

The column vector $\boldsymbol{f}$ of the node point stress corresponding to is as follows.

$$\boldsymbol{f} = \{m_t, z_i, z_j, z_k\}^T \qquad (2.5)$$

Here z_i, z_j, z_k are the node point stres in direction Z of points i, j, k, and m_t is the torque applied to the triangular element.

Next, w is solely dependent on x,y, as shown in equation (2.3), and so it is assumed to be as follows.

$$w = \alpha_1 + \alpha_2 x + \alpha_3 y \tag{2.6}$$

Since this calculation given above is carried out in the same way as an ordinary rigidity matrix [4], only the results will be shown.

$$\begin{Bmatrix} \theta \\ w_i \\ w_j \\ w_k \end{Bmatrix} = \begin{bmatrix} 1, & 0, & 0, & 0 \\ 0, & 1, & x_i, & y_i \\ 0, & 1, & x_j, & y_j \\ 0, & 1, & x_k, & y_k \end{bmatrix} \begin{Bmatrix} \theta \\ \alpha_1 \\ \alpha_2 \\ \alpha_3 \end{Bmatrix} = d = T\alpha \tag{2.7}$$

$$\begin{Bmatrix} \theta \\ \alpha_1 \\ \alpha_2 \\ \alpha_3 \end{Bmatrix} = \frac{1}{2A} \begin{bmatrix} 2A, & 0 & , & 0 & , & 0 \\ 0 & , x_j y_k - x_k y_j, & x_k y_i - x_i y_k & , x_i y_j - x_j y_i \\ 0 & , y_j - y_k & , & y_k - y_i & , & y_i - y_j \\ 0 & , x_k - x_j & , & x_i - x_k & , & x_j - x_i \end{bmatrix}$$

$$\begin{Bmatrix} \theta \\ w_i \\ w_j \\ w_k \end{Bmatrix}, \quad \text{or} \quad \alpha = T^{-1} d \tag{2.8}$$

Here A is the area of the base of the triangular element.

The Relation between Distortion and a

$$\varepsilon_x = \varepsilon_y = \varepsilon_z = \gamma_{xy} = 0$$

$$\gamma_{xz} = \frac{\partial u}{\partial z} + \frac{\partial w}{\partial x} = -\theta_y + \alpha_2$$

$$\gamma_{yz} = \frac{\partial v}{\partial z} + \frac{\partial w}{\partial y} = \theta x + \alpha_3$$

ORIGINAL PAGE IS
OF POOR QUALITY

That is, /6

$$\begin{Bmatrix} \gamma_{xz} \\ \gamma_{yz} \end{Bmatrix} \begin{bmatrix} y, & 0, & 1, & 0 \\ x, & 0, & 0, & 1 \end{bmatrix} \begin{Bmatrix} \theta \\ \alpha_1 \\ \alpha_2 \\ \alpha_3 \end{Bmatrix}, \quad e = B\alpha \tag{2.9}$$

The Relation between Stress and Distortion

G = shearing elasticity constant

$$\begin{Bmatrix} \tau_{xz} \\ \tau_{yz} \end{Bmatrix} = G \begin{bmatrix} 1 & 0 \\ 0 & 1 \end{bmatrix} \begin{Bmatrix} \gamma_{xz} \\ \gamma_{yz} \end{Bmatrix} \quad , \quad \sigma = D\varepsilon \qquad (2.10)$$

The Rigidity Matrix $[K^e]$

$$(K^e) = \iiint (N^T D N)\, dx\,dy\,dz = \iint (N^T D N)\, dx\,dy \qquad (2.11)$$

Here $N = BT^{-1}$

Table 2 shows the components of $[K^e]$.

TABLE 2. ELEMENT RIGIDITY MATRIX $(K^e) = (K_{ij})$

i \ j	1	2	3	4
1	$\frac{G}{4A}\{(y_j - y_k)^2 + (x_j - x_k)^2\}$	$\frac{G}{4A}\{(y_j - y_k)(y_k - y_i) + (x_j - x_k)(x_k - x_i)\}$	$\frac{G}{4A}\{(y_j - y_k)(y_i - y_j) + (x_j - x_k)(x_i - x_j)\}$	$\frac{G}{2}\{(y_k - y_i)y_0 + (x_k - x_j)x_0\}$
2		$\frac{G}{4A}\{(y_k - y_i)^2 + (x_k - x_i)^2\}$	$\frac{G}{4A}\{(y_k - y_i)(y_i - y_j) + (x_k - x_i)(x_i - x_j)\}$	$\frac{G}{2}\{(y_i - y_k)y_0 + (x_i - x_k)x_0\}$
3	対称		$\frac{G}{4A}\{(y_i - y_j)^2 + (x_i - x_j)^2\}$	$\frac{G}{2}\{(y_j - y_i)y_0 + (x_j - x_i)x_0\}$
4				$AG\{(y_0^2 + x_0^2) + \frac{1}{12}\{(y_i - y_0)^2 + (y_j - y_0)^2 + (y_k - y_0)^2 + (x_i - x_0)^2 + (x_j - x_0)^2 + (x_k - x_0)^2\}\}$

Here A = triangular area
G = shearing elasticity constant

$$x_0 = \frac{1}{3}(x_i + x_j + x_k) \quad , \quad y_0 = \frac{1}{3}(y_i + y_j + y_k)$$

Method of Torsional Analysis over all Cross Sections

By rearranging and combining the triangular element rigidity matrix to be found in Table 2, a rigidity matrix for all cross sections may be obtained. In this case all finite element rigidity

matrices cintain the same displacement component θ, which differs from the general case.

The equation for rigidity over all cross sections becomes as follows.

$$\begin{Bmatrix} z_1 \\ z_2 \\ z_3 \\ \vdots \\ z_n \\ \cdots\cdots \\ M_t \end{Bmatrix} = \begin{bmatrix} & \vdots & \\ [K_A] & \vdots & [K_{AB}] \\ & \vdots & \\ \cdots\cdots & \cdots\cdots & \cdots\cdots \\ [K_{AB}]^T & \vdots & K_B \end{bmatrix} \begin{Bmatrix} w_1 \\ w_2 \\ w_3 \\ \vdots \\ w_n \\ \cdots\cdots \\ \theta \end{Bmatrix} \qquad (2.12)$$

Here $M_t = \sum_{i=1}^{n} m_i$ becomes the torque over all cross sections.

When $\{z\} = \{z_1, z_2 \cdots z_n\}$, $\{w\} = \{w_1, w_2 \cdots w_n\}$, then from equation (2.12)

$$\{z\} = [K_A]\{w\} + \theta\{K_{AB}\} \qquad (2.13)$$

and since there is no external force applied in the Z direction

$$\{z\} = 0 \qquad (2.14)$$

and consequently (2.13) becomes

$$-\theta\{K_{AB}\} = [K_A]\{w\} \qquad (2.15)$$

and from (2.12) one obtains the following equation for M_t and . /7

$$M_t = \{K_{AB}\}^T\{w\} + K_B\theta = (\{K_{AB}\}^T\{\frac{w}{\theta}\} + K_B)\theta \qquad (2.16)$$

Solving equation (2.15) for $\frac{w}{\theta}$ and inserting the result in equation (2.16) one can calculate θ.

2.4 Bending Rigidity

The two dimensional moments over the cross sections of the models of Table 1 are obtained by calculating individually for the triangular elements then adding them at the center of gravity coordinates over the whole cross section.

In triangular element ABC (Figure 7), take the center of gravity G as the point of generation and consider a local coordinate system x,y in relation to the X axis parallel to the base.

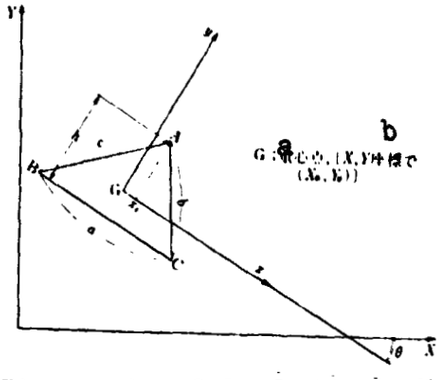

Figure 7. Calculation of two dimensional cross section moment for triangular element ABC.

The two dimensional cross section moment in relation to the X,Y coordinates becomes as follows.

$$I_{xx} = \int_{\triangle ABC} y^2 \, dA = \frac{A_0 h^2}{18}$$

$$I_{yy} = \int_{\triangle ABC} x^2 \, dA = A_0 \times \frac{(a^2 + b^2 + c^2) - 2h^2}{36}$$

$$I_{xy} = \int_{\triangle ABC} xy \, dA = A_0 \times \frac{x_A h}{12}$$

Here $A_0 = \frac{ah}{2}$, dA is differential area

Transform the above equations in terms of the basic X,Y coordinate system.

$$I_{XX} = I_{xx}\cos^2\theta + I_{yy}\sin^2\theta - 2I_{xy}\sin\theta\cos\theta + A_0 Y_0^2$$

$$I_{YY} = I_{xx}\sin^2\theta + I_{yy}\cos^2\theta + 2I_{xy}\sin\theta\cos\theta + A_0 X_0^2$$

$$I_{XY} = (I_{yy} - I_{xx})\sin\theta\cos\theta + I_{xy}(\cos^2\theta - \sin^2\theta) + A_0 X_0 Y_0$$

The center of gravity for all cross sections was taken as the point of generation of the basic coordinate system. Since the models of Figure 4 are symmetrical about the Y axis, the X and Y axes become inertial shafts.

3 Construction of Data for Applied Force

The model of Figure 3 is divided into blocks as in Figure 8.

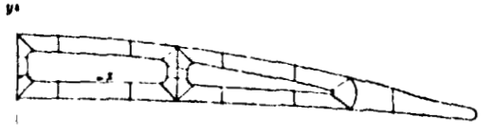

Figure 8. Example of the division of a model into blocks.

The blocks are simple connected territories made up from four or more node points. These blocks are transformed into square regions using a suitable mapping function. Thus Figure 9(a) is transformed into Figure 9(b). The black dots along the sides indicate the node points. Normally, on being transformed into a square, the left and lower

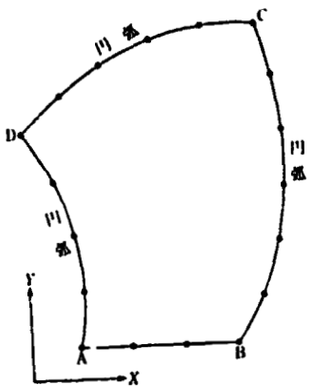

Figure 9(a). Example of automatic division

Key: a arc

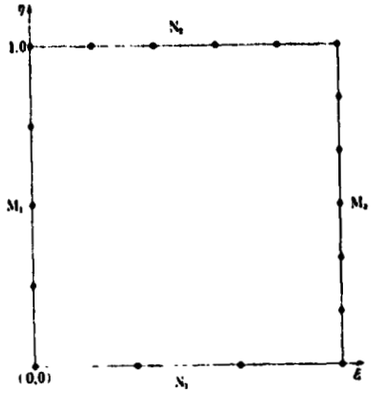

Figure 9(b). Mapping of a block on planes η and ξ.

sides will have fewer node points than the opposite sides. When /8
N_1, M_1, N_2, M_2 respectively represent the numbers of node points on the sides,

$$N_1 < N_2 , \quad M_1 < M_2$$

In order to divide the above squares into the required triangles, use the following procedure.

(1) Divide the block into $(N_1-1)X(M_1-1)$ smaller blocks by lines drawn through the node points on the left and lower sides (refer to Figure 9(c)).

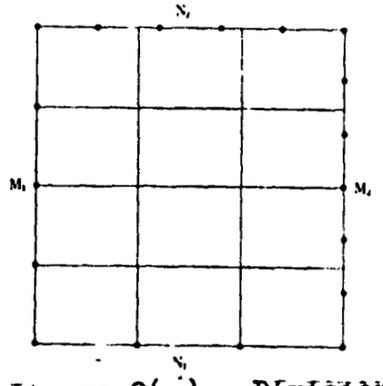

Figure 9(c). Division of a block by vertical and horizontal lines.

(2) Divide the horizontal lines by provisional node points as if the as if the node points increased directly from N_1 to N_2 (in Figure 9(d) shown by o). Divide the vertical lines in the same way with provisional node points as if they increased directly from M_1 to M_2 (in Figure 9(e) shown by x).

(3) The provisional node points on both the horizontal and vertical lines are shown simultaneously in Figure 9(f).

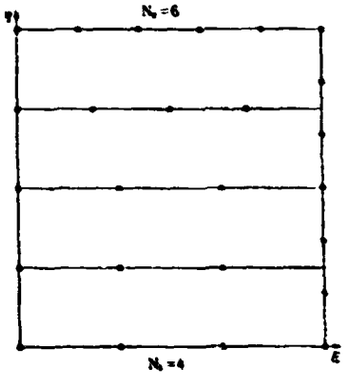

Figure 9(d). Distribution of provisional node points on horizontal lines (=1/4, 1/2, 3/4).

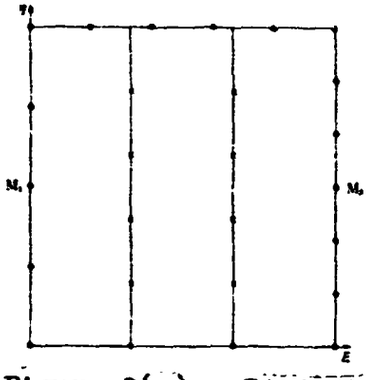

Figure 9(e). Distribution of provisional node points on vertical lines (= 1/3, 2/3).

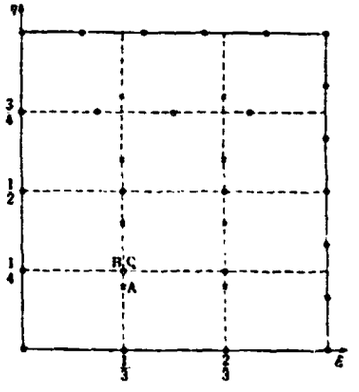

Figure 9(f). Distribution of provisional node points.

There are 7 provisional node on this diagram with the symbol o, and 8 provisional node points with the symbol x. There are 6 intersections between the vertical and horizontal lines. Combine the o symbol and the x symbol provisional node points closest to an intersection of the vertical and horizontal lines to make one real node point (calculate distance in terms of the original X,Y plane).

In Figure 9(f), the provisional /9 node points closest to intersection Q are A and B (by chance, B and Q coincide), and take their coordinates as A (ξ_A, η_A), B (ξ_B, η_B) whereupon the coordinates of the new real node point become (ξ_B, η_A). In this case the new real node point coincides with A. The intersection point between vertical and horizontal lines Q is moved to the real node point.

In Figure 9(g), scanning the intersection points starting in the lower left corner, determine the real node point x for intersection U, the third one. Provisional node points C and S are combined to form x. Since intersection point U is moved to x, provisional node point D, and so on, is moved to D', and so on, on the new horizontal line. Provisional node point T is moved to T' where it becomes the real node point. The remaining uncombined provisional node

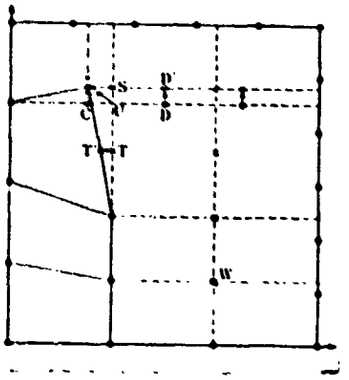

Figure 9(g). Determination of real node points.

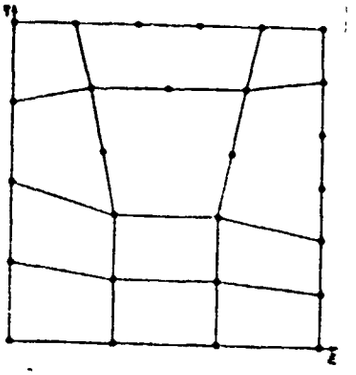

Figure 9(h). First division into blocks.

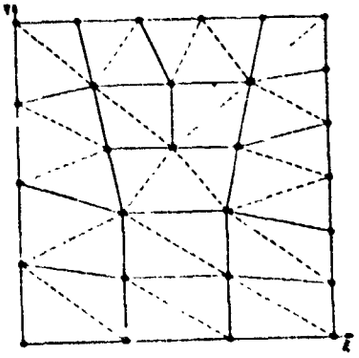

Figure 9(i). Final division into blocks.

points become real node points on the sides. Move intersection W by the same operation.

(4) Figure 9(h) is the situation when these operations have been completed for all intersections. The original block has been divided into 12 smaller blocks. Next repeat steps (1)-(3) for each small block wherever it is possible to carry out this kind of subdivision (where M_1 and N_1 are greater than 2).

(5) When the above blocks cannot be further subdivided, divide these blocks into triangles (Figure 9(i)). Choose the shortest paths for the dividing diagonal lines.

When the division of the block is completed as above, return it to its original form by reverse mapping (see Figure 9(j)).

This method has the following advantages compared to the older methods [5,6].

(i) It is not necessary for node points on opposite sides to be equal in number.

(ii) As seen in Figure 9(j) the dividing lines are bent and bias in the dividing pattern is slight.

However, because of the following limitations further improvement is necessary.

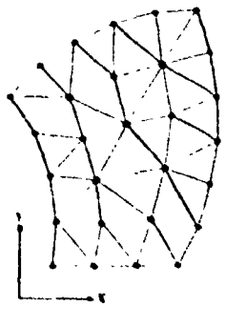

Figure 9(j). Completion of the automatic subdivision returned to the X,Y plane by reverse mapping (28 node points, 36 elements).

When the density of the distribution of node points on a given side is such that it becomes uneven, a bias is developed in the distribution pattern when the method of distributing provisional node points using straight lines is used.

The entry of data is in a free format form, since there is little data and it can be understood at a glance. The entry of data for the example presented above is shown as Figure 8(a).

4 Results of the Analysis

/10

The results of the analysis are given in Table 3.

```
(1)  AUTO PARTITION EXAMPLE                    title
(2)  A-0.0. 0.0
(3)  B-3.0. 0.0                                node point name and co-
(4)  C-3.5. 6.0                                ordinate data
(5)  D--1.0. 4.0
(6)  A>B-3
(7)  B>C-6/4.0. 3.0                            state of sides and number of
(8)  C>D-5/1.0. 5.5                            divisions
(9)  D>A-4/0.0. 2.0
(10) UNIT/NO. 1-A/B/C/D                        definition of block no. 1
(11) END                                       end of data
```

Figure 8(a). Entry list for example of automatic division.

Data entries 7 - 9 show that the sides are arcs. The arc is defined by the end points and the point whose coordinates are given after the /.. The entries are in a free format form.

4.1 Rigidity

Torsional rigidity in the table, J, is a value defined by the following equation.

$$M_z = JG\theta$$

Here M_z is torque (kg-m)

J is torsional rigidity (m-mm/rad)

G is shearing elasticity constant (kg/mm)

θ is torsion percentage (per unit length) (rad/mm)

30% hollowing produces about a 13-16% decrease in torsional rigidity compared to a solid blade, but per unit area hollowing produces a 20-24% increase in torsional rigidity. We think this result from hollowing satisfactory. With a 30% hollowed cylinder taken as the ideal case, the torsional rigidity per unit area would increase 30%.

TABLE 3. RESULTS OF THE ANALYSIS

Model 2	Dimension Bending Moment I	Torsional Rigidity J	Torsional Rigidity per Unit area	Greatest Displacement in Direction of Axis	Greatest Shearing Stress
Solid	1118.88 kg^2	3.060 $m-m^2/rad$	0.8336 $\times 10^{-2}$ $m-m^2/rad$	0.3581 $\times 10^{-1}$ m	6.460 kg/mm^2
0A	996.58	2.548	0.9956	0.4622	8.0*
0B	988.70	2.609	1.018	0.4521	7.564
1A	1004.68	2.552	0.9992	0.4629	7.775
2A	989.94	2.585	1.019	0.4498	7.905
Opt	1020.38	2.661	1.034	0.4588	7.337
3A	996.76	2.611	1.013	0.4407	8.220
3B	990.38	2.636	1.020	0.4415	8.005
3C	993.28	2.660	1.031	0.4400	7.679
7A	990.72	2.592	0.9942	0.4499	8.229

Mt = 3.65 kg-m

*inferred from stress distribution

The two dimensional cross section moment decreases 10-11% but is increased 27-29% per unit area. In the case of bending rigidity the results obtained were higher than for torsional rigidity, because of the difference in the stress distributions.

The reinforcing webs had no influence on torsional rigidity or bending rigidity. As related below, the webs have the effect of breaking up concentrations of stress and their influence on such large scale values as rigidity is slight. However, properly located, they increase the torsional rigidity per unit area about 5%. For any cross section area (that is, percentage of hollowing) attachment of a web causes two opposing tendencies with respect to torsional rigidity, a balance between one which increases resistance to displacement along the axis established by the reinforcing web, and another which lowers strength because of the decrease in thickness of the blade surface material. The cases of 2 or 3 webs gave the highest rigidity, compared to either 0 or 7 webs. And, locating the webs near the ends gave better results than locations in the center.

The torsional distortion of a hollow blade is shown in Figure 10. In the figure the distortion is greatly exaggerated. There is a slippage between the distortion of the upper and lower plates

ORIGINAL PAGE IS
OF POOR QUALITY

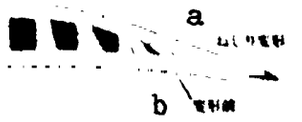

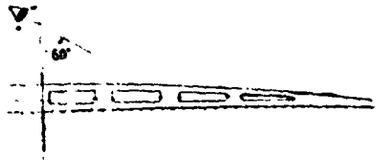

Figure 10. Torsional distortion of a hollow blade (model 7A) (view of a cross section of the blade at an angle of 60%)

Key: a torsional distortion

b before distortion

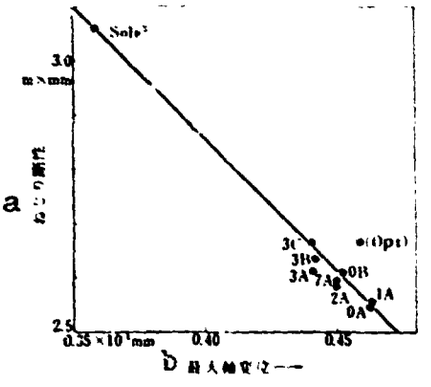

Figure 11. Greatest axial distortion and torsional rigidity.

Key: a torsional rigidity

b greatest axial distortion

in the direction of the axis, and because of this there is a shearing distortion in the direction of the axes of the webs. The distortion of the lower plate is considerable. Overall the tips of the hollow blades /11 show the greatest axial displacement. The relationship between this greatest distortion and torsional rigidity is shown in Figure 11. The general trend is a linear relationship between torsional rigidity and greatest distortion in the axial direction, the less the axial distortion, the greater the torsional rigidity.

Because of this it is felt that an oblique web configuration as in Figure 12 would be the most successful.

The role of the webs in the case of the parallel webs analyzed here is principally, as seen in Figure 10, to resist distortion in the direction of the axis in the upper and lower plates of the blade. That is, to the extent that there is a differential distortion between the upper and lower plates, the webs will come under a load and move. In the center part, because of symmetry, there is no difference in distortion, but this increases approaching the tips, then becomes zero at the spot where the upper and lower plates meet. The location where parallel webs will have the greatest effect is near this area.

OF POOR QUALITY

Figure 12. Reinforcement by oblique webs.

4.2 Concerning the Distribution of Stresses

The flow of overall shearing stress $\tau=\sqrt{\tau_{xz}^2+\tau_{yz}^2}$ is shown in Figure 13(a)-(e). The direction arrows in the figures are plotted for each element and show the direction of the slow of shearing stress at the center of gravity of each element. The size of the arrows is fixed. The density of the arrows has no relation to the magnitude of the shearing stress. /12

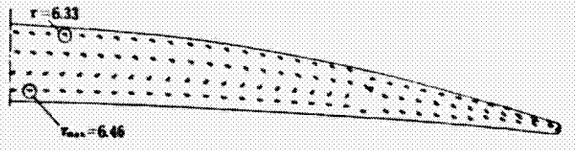

Figure 13(a). The flow of shearing stress in the solid model.

In the case of the webless model (OA) the greatest shearing stress was found at point A, near the tip of the hollow section (see Figure 13 (b)).

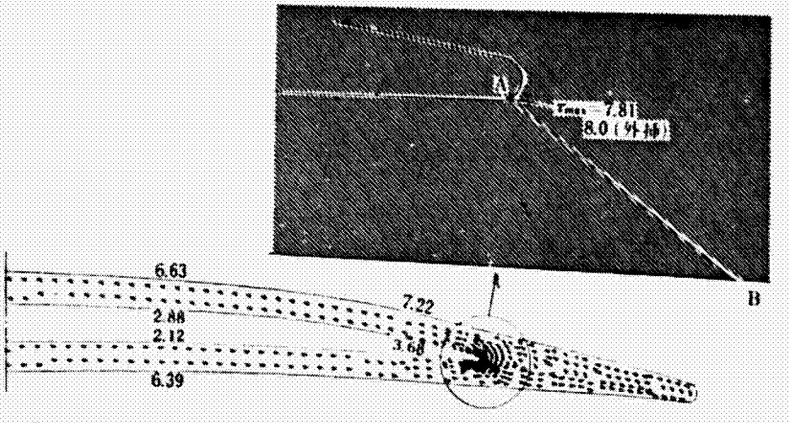

Figure 13(b). The flow of shearing stress in model OA.

The distribution of stress over the cross section AB is shown in Figure 14.

The stress distribution, highest at point A, decreases with passage into the interior region and increases again near point B.

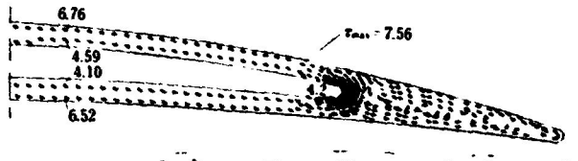

Figure 13(c). The flow of shearing stress in model OB.

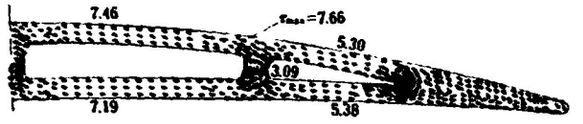

Figure 13(d). The flow of shearing stress in model 3B.

Figure 13(e). The flow of shearing stress in model 7A (interior lines abbreviated).

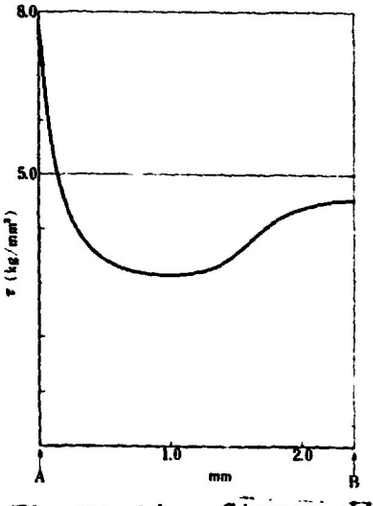

Figure 14. Stress distribution in the region near the tip of the hollow section (model OA).

The increase near point B is normally seen in torsional stress. It is thought to be a consequence of the addition of the concentrated stresses about point A in this kind of stress distribution curve (radius of curvature ρ = 0.2mm).

In the case of model OB, where the radius of curvature ρ = 0.5mm, the concentration of stresses at point A is lower and the maximum stress is produced elsewhere.

When a web is added the stresses are divided and flow in the direction of the web, so that a lowering of stress near the tip of the hollow section is seen.

The concentration of stresses at the point of junction between the webs and the upper and lower plates is low in the present models (round, radius 0.6mm) and there are no problems with their intensity.

The flow of shear stress within the webs, as seen in the 7 web model (Figure 13(d)), forms eddies in the central webs and flows along the webs near the tip. The shearing stress within the webs is low.

5 Discussion

The effect of the webs on torsional rigidity is, as shown in Figure 10, to lower the difference in distortion in the axial direction of the upper and lower plates. We have discovered the location where this effect is greatest.

Consider the model (OA) in which no webs at all are introduced. When the model is subjected to torque there is distortion. The vertical cross section of this model at a location x mm removed from the center of the chord along the X axis is shown in Figure 15. If we consider the two planes 1 mm apart which are emphasized in the figure (shown by broken lines in the figure), a point located at just the distance between planes will be displaced by exactly $x\theta$. The value of the angle of rotation of the planes $\Delta\omega/l$ (l = the distance between the upper and lower plates of the blade) which is derived from this displacement value is the shearing distortion (r) of the hypothetical web, and so

$$r = x\theta - \frac{\Delta\omega}{l} \qquad (5\text{-}1)$$

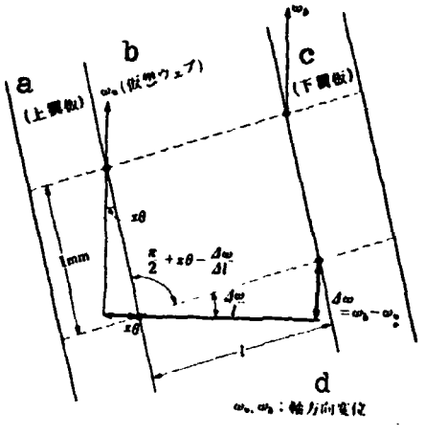

Figure 15. Shearing distortion in a hypothetical web. (vertical cross section x mm from the center).

Key: a upper plate
b hypothetical web
c lower plate
d displacement in direction of axis

In fact there is also produced a torsional distortion amounting to just θ in this hypothetical web, but because this is uniform over the cross section it is reasonable to disregard it in this analysis.

The final result of the calculations for model (OA) using all the above equations is shown in Figure 16.

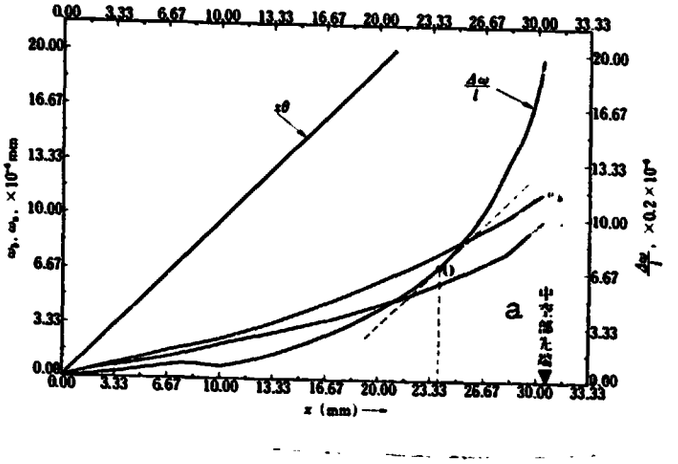

Figure 16. Bending and the displacement between upper and lower plates of blade model OA.

Key: a tip of hollowed section

Point O, where equation (5-1) is greatest, is the point of intersection of the intersecting curved lines running parallel to the straight line $x\theta$. This location is comparatively near the end of the hollowed section, and this agrees with the tendency of the results of torsional rigidity analysis for each model tested so far. In the center section the webs show only the most slight effects. /13

When we place a web at point O (though strictly we do not use data from model OA) we consider that the web will bear the greatest shearing distortion (and so the rigidity will be highest).

The optimum model is the one where the webs are placed at point O. From Table 2 the torsional rigidity per unit area is highest, and becuase the nubmer of webs is small, the thickness of the upper and lower plates is increased and both bend rigidity and greatest shearing stress are improved.

In dealing with torsional rigidity by the above outlined method it is necessary to consider 1) overall analysis by some effective method (i.e. a method covering all stresses) which takes account of changes in the thickness of the upper and lower plates, and 2) employment of oblique webs as in Figure 12. However, one should expect no great improvement over the present 24% increase, in light of the 30% increase in torsional rigidity (per unit area) in the case of a hollow cylinder.

The study of bending and external loadings is important. For example, while central webs are unnecessary in relation to torsion, they are assumed valuable in relation to external loadings. /14

Examined from the perspective of stresses, the greatest stress with 30% hollowing is less than 10 kg/mm^2, and so hollowing to about 30% is considered fully possible in relation to hypothesized torsional loadings.

6 Conclusions

In order to study hollow fan blades, light in weight yet high in trustworthiness in terms of structural strength, for use in aircraft fan jet engines, we took as examples certain experimental fan blades and obtained the following results from analysis of torsional stress and rigidity for hollowed models of them.

1) Hollowing by 30% reduced torsional rigidity by 13-16% and bending rigidity by 10-11%. The maximum shearing stress was increased 17-27%. However, when computed in relation to unit area, torsional rigidity increased 20-24%.

2) Reinforcing webs had a negligible effect on torsional rigidity but a good effect on the compounding of stresses.

3) As for the location of webs, when placed where the shearing distortion within the webs are greatest, there is a good effect on torsional rigidity.

4) By selecting an appropriate configuration of hollowing a weight saving of 30% is possible allowing for all anticipated torsional loadings.

REFERENCES

1. Miyaji et al, "Concerning vibration in the blades of axial flow rotary machines," Aeronautical Research Report TR-176.

2. For example, Timoshenko et al, Theory of Elasticity.

3. Kawai, T. and Yoshimura, N., "Torsional analysis of a bar by the matrix method," Seisan Kenkyū 20/5, 52-54.

4. For example, Zienkiewicz, O.C., Matrix Yūgen Yōso Hō [The Matrix Finite Element Method], Baifūkan, Tokyo, 1975.

5. Zienkiewicz, O.C. et al, "An automatic mesh generation scheme for plane and curved surfaces by isoparametric co-ordinates," International Journal for Numerical Methods in Engineering 3, 519-528 (1971).

6. Hayashi, Y., "A technique of automatic element division for use with the finite element method (plane construction)," Mitsubishi Jūkō Gihō 9/5, 649.

7. Fujii, et al, "The development of the study of front fans," Aeronautical Research Reference TM-290.